A motion estimation and compensation algorithm for 4D CBCT of the abdomen

Seongjin Yoon[a], **Alexander Katsevich**[a,b,*], **Michael Frenkel**[a], **Peter Munro**[c], **Pascal Paysan**[c], **Dieter Seghers**[c], **Adam Strzelecki**[c]
[a]iTomography Corp., Texas Medical Center Innovation Institute, 2450 Holcombe Blvd, Houston, TX 77021, USA
[b]University of Central Florida, Mathematics Department, Orlando, FL 32816, USA
[c]Varian Medical Systems Imaging Laboratory, Taefernstrasse 7, 5405 Daettwil, Switzerland

Abstract. We propose an algorithm for periodic motion estimation and compensation in the case of a slowly rotating gantry, e.g., as is the case in cone beam CT. The main target application is abdomen imaging, which is quite challenging because of the absence of high-contrast features. The algorithm is based on minimizing a cost functional, which consists of the data fidelity term, the optical flow constraint term, and regularization terms. To find the appropriate solution we change the constraint strength and regularization strength parameters during the minimization. Results of experiments with simulated and clinical data demonstrate promising performance.

Keywords: motion estimation, motion compensation, optical flow constraint, changing regularization strength, abdomen imaging.

*Alexander Katsevich, alexander@itomography.com

1 Introduction

Image reconstruction using on-board cone-beam computed tomography (CBCT) is an important component of image-guided radiotherapy (IGRT) workflow. Due to the slow rotation of the gantry, motion estimation and compensation become critically important. A number of algorithms for solving this problem have been proposed (see e.g., Ref. 1–3 and references therein). Since the slowly rotating gantry does not collect sufficient amount of time resolved projection data, most of these algorithms work well only in regions of the patient that contain high-contrast features, e.g., the chest, and fail in relatively homogeneous regions. Imaging of the abdomen is especially challenging, since very few high-contrast features are present there. Iterative reconstruction algorithms based on enforcing the optical flow constraint appear to be most powerful (see Ref. 4 for convergence analysis) and can potentially provide clinically acceptable image quality in the abdomen. In this paper, we propose one such algorithm and test it on simulated and clinical data. The novel idea is that we change parameters of the cost functional in a dynamic fashion during optimization to steer the algorithm towards a solution with required properties, e.g., with reduced sparse view streaks. We performed tests on simulated and clinical data, but presented here only one clinical example. Our tests demonstrated that the proposed algorithm provides good image quality, allows to identify low-contrast features with accuracy sufficient for clinical applications.

2 Description of the algorithm

2.1 High level algorithm outline

Let s be the time variable. The dynamic object is represented by a function $f(s,\vec{x})$ and periodic deformation $\vec{\psi}(s,\vec{x})$ so that $f(s,\vec{x}) = f_0(\vec{\psi}(s,\vec{x}))$ and $\psi(s,\vec{x}) = \psi(s+T,\vec{x})$. Here, $f_0(\vec{x})$ is the

15th International Meeting on Fully Three-Dimensional Image Reconstruction in Radiology and Nuclear Medicine, edited by Scott D. Metzler, Samuel Matej, Proc. of SPIE Vol. 11072, 110720E · © 2019 SPIE · CCC code: 0277-786X/19/$18 · doi: 10.1117/12.2534879

attenuation coefficient at reference time, and T is the period of motion. The optical flow constraint is given by

$$\frac{\partial f(s,\vec{x})}{\partial s} + \nabla f(s,\vec{x}) \cdot \vec{v}(s,\vec{x}) = 0, \tag{1}$$

where $\vec{v}(s,\vec{x})$ is the velocity vector at $\vec{x}$ at time s. Let s_m, $0 \leq m < M$, be the collection of times corresponding to the measured views, and $\mathcal{L}_{mk}$, $0 \leq k < K$, be the collection of lines corresponding to the mth source position. In other words, $\mathcal{L}_{mk}$ is the line through the mth source position and the kth detector pixel. The measured data are denoted G_{mk}. To solve the motion estimation and compensation problem, we find $f(s,\vec{x})$ and $\vec{v}(s,\vec{x})$ by minimizing the following functional:

$$\begin{aligned}\Phi(f,\vec{v}) =& \frac{1}{2}\sum_{mk} w_{mk}\left[G_{mk} - \int_{\mathcal{L}_{mk}} f(s_m,\vec{x})\mathrm{d}\ell\right]^2 \\ &+ \frac{\lambda}{2}\int\int_0^T \left[\frac{\partial f(s,\vec{x})}{\partial s} + \nabla f(s,\vec{x})\cdot\vec{v}(s,\vec{x})\right]^2 \mathrm{d}s\,\mathrm{d}\vec{x} + (\text{regularizers for } f \text{ and } \vec{v}).\end{aligned} \tag{2}$$

Here, $\lambda > 0$ needs to be large enough to enforce the optical flow constraint (1). We assume that the dynamic object f is less smooth than the velocity $\vec{v}$. Hence, we use an edge-preserving regularizer for f (the hyperbolic potential), and the Tikhonov regularizer for $\vec{v}$. We use a method of alternating minimization to demonstrate the performance of the proposed algorithm.

2.2 Alternating minimization and dynamic parameter selection

Suppose the reconstruction volume and the motion grids are given by

$$\vec{x}_{\mathbf{i}} = (h_1 i_1, h_2 i_2, h_3 i_3),\ \mathbf{i} = (i_1,i_2,i_3),\ \text{ for } 0 \leq i_q < N_q,\ q = 1,2,3, \tag{3}$$

$$\vec{m}_{\mathbf{j}} = (\tilde{h}_1 j_1, \tilde{h}_2 j_2, , \tilde{h}_3 j_3),\ \mathbf{j} = (j_1,j_2,j_3),\ \text{ for } 0 \leq j_q < \tilde{N}_q,\ q = 1,2,3. \tag{4}$$

For all $\vec{x}$, we have $f(s,\vec{x}) \approx \sum_{\mathbf{i}} f_{\mathbf{i}}(s)\varphi_h(\vec{x}-\vec{x}_{\mathbf{i}})$, and $\vec{v}(s,\vec{x}) \approx \sum_{\mathbf{j}} \vec{v}_{\mathbf{j}}(s)\widetilde{\varphi}_h(\vec{x}-\vec{m}_{\mathbf{j}})$, where φ_h and $\widetilde{\varphi}_h$ are interpolation kernels for volume and motion grids, respectively. To enforce smoothness of the motion vector field (MVF), we select $\tilde{h}_q \gg h_q$ and $\tilde{N}_q \ll N_q$, and use the linear interpolation kernel for the volume grid (φ_h), and the cubic B-spline kernel for the motion grid ($\widetilde{\varphi}_h$). Let there be N_p discrete phase bins. Let $\mathbf{f}$ and $\mathbf{v}$ denote phase volumes and MVFs unrolled into 1D vectors, respectively. Then, we discretize (2) with respect to s and rewrite it in a matrix-vector form as follows:

$$\Phi(\mathbf{f},\mathbf{v}) = \Phi_{\mathrm{L}}(\mathbf{f}) + \lambda\Phi_{\mathrm{fv}}(\mathbf{f},\mathbf{v}) + \kappa_f\Phi_{\mathrm{R_f}}(\mathbf{f}) + \kappa_v\Phi_{\mathrm{R}_v}(\mathbf{v}), \tag{5}$$

where $\Phi_{\mathrm{L}}(\mathbf{f})$ is the data fidelity functional (as used in the PWLS approach), $\Phi_{\mathrm{fv}}(\mathbf{f},\mathbf{v})$ is the optical flow constraint, $\Phi_{\mathrm{R_f}}(\mathbf{f})$ is the volume regularizer, and $\Phi_{\mathrm{R}_v}(\mathbf{v})$ is the velocity regularizer defined as:

$$\Phi_{\mathrm{L}}(\mathbf{f}) := \frac{1}{2}(\mathbf{G}-\mathbf{A}\mathbf{f})^{\mathsf{T}}\mathbf{W}(\mathbf{G}-\mathbf{A}\mathbf{f}), \quad \Phi_{\mathrm{fv}}(\mathbf{f},\mathbf{v}) := \frac{1}{2}\left\|\mathbf{D}\mathbf{f} + \sum_q \mathrm{diag}\left\{\mathbf{B}\mathbf{v}_q\right\}\mathbf{C}_q\mathbf{f}\right\|_2^2, \tag{6}$$

$$\Phi_{\mathrm{R_f}}(\mathbf{f}) := \sum_q \sum_{\mathbf{i}} \phi_{\mathrm{R}}([\mathbf{C}_q\mathbf{f}]_{\mathbf{i}},\ \delta),\quad \Phi_{\mathrm{R}_v}(\mathbf{v}) =: \frac{1}{2}\sum_q \sum_r \sum_{\mathbf{j}} \Big([\mathbf{C}_r\mathbf{v}_q]_{\mathbf{j}}\Big)^2. \tag{7}$$

Here, $\mathbf{G}$ is the entire set of measured data, $\mathbf{f}$ is the entire set of phase volumes in vector form, $\mathbf{v}$ is the entire set of phase MVFs in vector form, $\mathbf{v}_q$ is the component of $\mathbf{v}$ along the qth axis, $\mathbf{A}$ is the system matrix, $\mathbf{W}$ is the weight matrix, $\mathbf{B}$ is the upsampling matrix (from the motion grid (4) to the volume grid (3)) based on cubic B-spline interpolation, $\mathbf{D}$ is the temporal finite difference matrix along the phase bins with periodic boundaries, $\mathbf{C}_q$ is the spatial finite difference matrix along the qth axis with clamped boundaries, $\mathrm{diag}\{\mathbf{t}\}$ is the diagonal matrix with the elements of vector $\mathbf{t}$ on the main diagonal, $\big[\mathbf{t}\big]_i$ is the ith element (scalar, vector, or matrix) along the first dimension of vector or matrix $\mathbf{t}$, $\phi_{\mathrm{R}}(t,\ \delta)$ is the hyperbolic potential regularizer. In general, $\mathbf{W}$ is derived from the raw projection data to account for relative noise intensity. For now, we set $\mathbf{W}$ as an identity matrix. Later, we are planning to use $\mathbf{W}$ to represent the phase-amplitude uncertainty. The dimension of $\mathbf{C}_q$ is determined by the vector to which it applies.

2.3 Method of Alternating Minimization with respect to Volume and Velocity

The total cost functional in (5) is nonlinear, nonconvex, and ill-conditioned. Minimizing (5) with respect to $\mathbf{f}$ and $\mathbf{v}$ simultaneously often falls into undesirable local minima. The method of alternating minimization helps in this case by splitting the problem into two simpler sub-problems and guiding the solution to the desired local minimum.

With the alternating minimization scheme, each global iteration consists of a set of volume sub-iterations and a set of MVF sub-iterations. The cost functional is minimized with respect to either $\mathbf{f}$ or $\mathbf{v}$ in an alternating fashion while keeping the other variable fixed. This way, each sub-problem becomes convex, which is easier to solve. Starting volume sub-iterations with a large λ when all phase MVFs are initialized as zero ends up underestimating the motion. In the extreme case, when $\lambda = \infty$, the reconstructed phase volumes are all the same at the end of the initial set of volume sub-iterations. Once motion information is lost, it is hard to recover the accurate motion in subsequent MVF sub-iterations. To appropriately utilize the optical flow constraint, we vary λ during the course of optimization.

On the other hand, angular sampling for each temporal bin is very low, so strict phase gating methods often create strong sparse view streaks that adversely affect MVF estimation. Hence we start global iterations with a small value of λ to avoid MVF underestimation and strong volume regularizer κ_f to reduce sparse view-sampling streaks. Then, we gradually ramp up λ, and simultaneously reduce κ_f to restore details. For example, we use the following values for λ and κ_f at each global iteration step n_{g} using parameters $\lambda_{\max}$, $\kappa_{\max}$, and $\kappa_{\min}$:

$$\lambda(n_{\mathrm{g}}) = \min\left(\lambda_{\max}\frac{n_{\mathrm{g}}+0.5}{N_{\mathrm{g}}-1}, \lambda_{\max}\right),\ \kappa_f(n_{\mathrm{g}}) = \max\Big(\kappa_{\max}2^{-n_{\mathrm{g}}}, \kappa_{\min}\Big), \tag{8}$$

where N_{g} is the total number of global iteration steps. While increasing λ during optimization is a well-known approach that is used to convert a constrained problem into an unconstrained one, the idea to reduce κ_f appears novel. In addition, the algorithm does not introduce any auxiliary

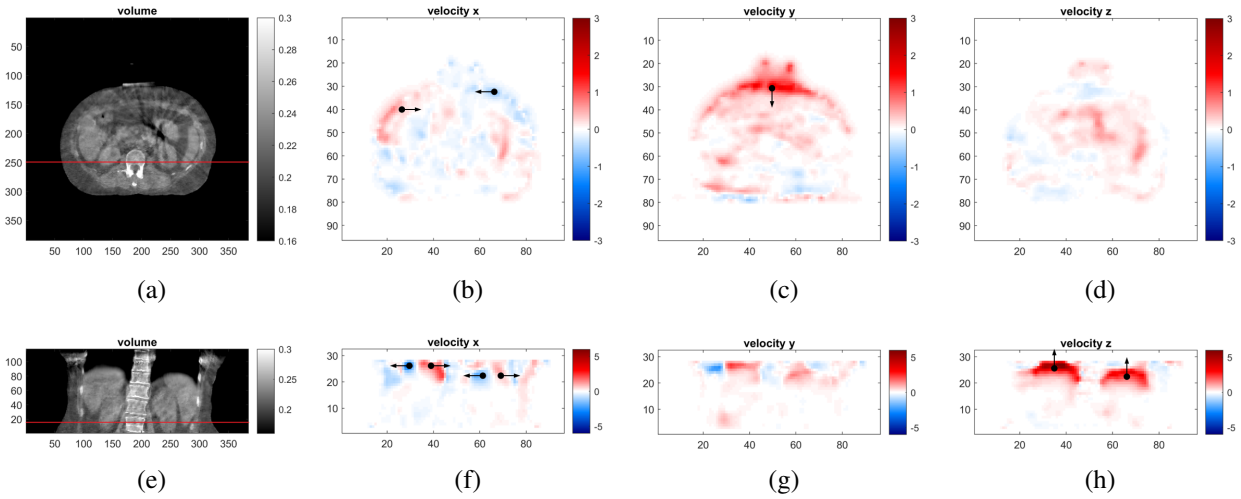

Fig 1 Cross-sections through the reconstructed volume $f(s, \vec{x})$ and MVF $\vec{v}(s, \vec{x})$ at the level of the kidneys for the clinical data: transverse view (a)-(d) and coronal view (e)-(h). Time s corresponds to the middle of the exhale. The red line in each volume slice shows the location of the opposite view. The unit of the velocity is pixels$/\Delta_{\text{phase}}$, where $\Delta_{\text{phase}} =$ respiratory cycle$/10$. Black arrows illustrate the direction of the major motion.

variables thereby reducing memory requirements (cf. Ref. 3, 4), and image registration becomes an implicit part of the optimization (cf. Ref. 3).

A preconditioner and Nesterov's momentum acceleration method Ref. 5 are applied to each sub-iteration step to increase the convergence speed. No acceleration of global iterations is applied due to the risk of overshooting and instability, since the overall functional is not convex.

3 Numerical Experiments

We present reconstruction results for a clinical dataset acquired using Varian TrueBeam® scanner with half-fan beam geometry. Chest motion amplitude was recorded using TrueBeam's respiratory gating system, and then converted to the breathing phase. Fig. 1 shows transverse and coronal cross-sections through the reconstructed object f and the corresponding MVFs of a clinical case. Additional reconstruction results from simulated and clinical data will be shown at the conference.

Results of numerical experiments show that ramping up λ and reducing κ_f during optimization significantly reduces sparse-view streak artifact, reduces motion underestimation, and preserves contrast resolution. As a result, low-contrast features that are normally very difficult to see in CBCT images can now be resolved. Future work will concentrate on evaluating the proposed algorithm using a large number of clinical data sets.

References

1 Z. Qi and G. Chen, "Performance studies of four-dimensional cone beam computed tomography," *Physics in Medicine and Biology* **56**, 6709–6721 (2011).

2 M. Brehm, P. Paysan, M. Oelhafen, *et al.*, "Artifact-resistant motion estimation with a patient-specific artifact model for motion-compensated cone-beam CT," *Medical Physics* **40** (2013). article id 101913.

3 H. Zhang, J. Ma, Z. Bian, *et al.*, "High quality 4D cone-beam CT reconstruction using motion-compensated total variation regularization," *Physics in Medicine and Biology* **62**, 3313–3329 (2017).
4 M. Burger, H. Dirks, and C.-B. Schoenlieb, "A Variational Model for Joint Motion Estimation and Image Reconstruction," *SIAM Journal on Imaging Sciences* **11**, 94–128 (2018).
5 Y. Nesterov, "A method of solving a convex programming problem with convergence rate $O(1/k^2)$," *Soviet Mathematics - Doklady* **27**, 372–376 (1983).